Journal of the European Ceramic Society 21 (2001) 999–1005

www.elsevier.com/locate/jeurceramsoc

Thermal shock resistance of α/β-sialon ceramic composites

Pernilla Pettersson, Zhijian Shen, Mats Johnsson *, Mats Nygren

Department of Inorganic Chemistry, Arrhenius Laboratory, Stockholm University, S-106 91 Stockholm, Sweden

Received 3 September 2000; accepted 16 October 2000

Abstract

The thermal shock properties of α/β-sialon composites have been evaluated with an indentation-quench method based on propagation of Vickers cracks. Nominally the z value of the β-phase ($Si_{6-z}Al_zO_zN_{8-z}$) was held constant at 0.6, and the composition of the α-sialon phase $Y_xSi_{12-(m+n)}Al_{m+n}O_nN_{16-n}$ was $x=0.33$, $m=1.0$, $n=1.2$. Different $\alpha/(\alpha+\beta)$ ratios were tested, and the amount of sintering aid (a yttrium-containing glass phase) was varied between 0 and 20 vol.%. The thermal shock resistance increases with increasing fraction of β-phase, and the presence of a glass phase also has a positive influence on the thermal shock resistance.

Keywords: Crack growth; Indentation; Sialons; Thermal shock resistance

1. Introduction

α- And β-sialons are two solid-solution phases with crystal structures isomorphous to α- and β-Si_3N_4, respectively. β-sialon is represented by the general formula $Si_{6-z}Al_zO_zN_{8-z}$, with $0<z\leqslant 4.2$, and α-sialon by $M_xSi_{12-(m+n)}Al_{m+n}O_nN_{16-n}$, where M is a metal ion (most often Y or a rare-earth element) and x, m, and n are parameters that restrict the formation of α-sialon to a small compositional area.[1] One obvious advantage of ceramics that consist of α- and β-sialon over monophasic silicon nitride is the possibility to tailor the microstructures in a more flexible way. This is because aluminium and other metal cations are involved in the system, which makes it possible to introduce a transient liquid to assist the densification and grain growth processes at the sintering temperature. The liquid phase disappears during the sintering process, as its constituents subsequently are incorporated into the sialon crystal structure. Thus, it is possible to prepare duplex α/β-sialon composites with a minimum amount of secondary intergranular glass phase by adjusting the overall α-β-sialon composition.

Previously this kind of composites has been prepared in yttria- and rare earth-doped systems.[2,3] By developing an in-situ reinforced microstructure consisting of needle-shaped well-distributed β-crystals in an α-sialon matrix, the obtained materials acquire a better combination of hardness and toughness than monophasic α- or β-sialon ceramics. The hardness is comparable to α-sialon, and the fracture toughness and high-temperature creep resistance are improved. These materials have attracted attention for high-temperature structural applications such as heat engine components and cutting tool inserts. Despite the improvement in hardness and fracture toughness, however, the cutting test unexpectedly showed that these materials had no obviously improved cutting performance. The subsequent standard failure analysis showed that the main failures were caused by cracks formed during thermal cycling, indicating the necessity for a better understanding of the thermal-shock properties of these materials.

At the moment, there are few experimental data available in the literature concerning the effect of thermal cycling on mechanical properties of sialon-based materials. A systematic study therefore seems necessary, exploring e.g. the relation between the microstructure, mechanical properties and the thermal shock behaviour of these materials. In this article we report the thermal-shock properties of α-β-sialon composites. Microstructural features such as the $\alpha/(\alpha+\beta)$ ratio and the amount of residual intergranular glass phase present are considered, and their effect on thermal shock behaviour is discussed.

Various methods have been developed over the years in order to measure the thermal shock resistance of a material. Most of those methods are based on test bars

* Corresponding author. Tel.: +46-8-674-70-67; fax: +46-8-15-21-87.

E-mail address: matsj@inorg.su.se (M. Johnsson).

0955-2219/01/$ - see front matter
PII: S0955-2219(00)00303-4

of specified dimensions and geometries, which are heated to thermal equilibrium in a furnace and then quenched into a water bath and subsequently subjected to mechanical testing, for example by determining their three- or four-point bending strength.[4–7] The manufacture of test bars with well-defined shape and surface finish is complicated and expensive. In addition, separate bars are required for each temperature to be tested, and several bars are used at each temperature to improve statistics. Those methods are thus both time-consuming and costly.

In an indentation–quench method developed by Andersson and Rowcliffe[8] small Vickers cracks are made on a cylinder with a thickness of 3–5 mm. The cylinder is then heated in a vertical tube furnace and subsequently quenched into a water bath; thereafter the crack growth is measured and correlated with the temperature difference. The method allows the same sample to be used through a series of temperatures,[9] and by measuring the growth for several Vickers cracks on the same sample the statistics is improved. This method was applied in the present work because it provides such an efficient way to determine and compare the thermal shock resistance of different materials.

2. Experimental

2.1. Sample preparation

Two series of samples named I and II were prepared, see Table 1. Samples of series I, with overall compositions located exactly on the α–β phase plane, were designed to give α–β-sialon composites with minimum amounts of secondary intergranular glass phase, assuming complete reaction to take place during densification. The α- and β-sialons were $Y_{0.33}Si_{9.8}Al_{2.2}O_{1.2}N_{14.8}$ ($x=0.33$, $m=1.0$, $n=1.2$) and $Si_{5.4}Al_{0.6}O_{0.6}N_{7.4}$ ($z=0.6$), chosen on the basis of previous experience.[10]

Table 1
Overall compositions of the starting materials (in wt.%)

Series I					
Sample	$\alpha/(\alpha+\beta)$	Y_2O_3	Si_3N_4	AlN	Al_2O_3
B06	0	–	90.41	5.29	4.33
ABY20	0.2	1.3	88.00	7.10	3.60
ABY30	0.3	1.9	86.80	8.00	3.30
ABY50	0.5	3.2	84.40	9.80	2.60
ABY100	1.0	6.3	78.30	14.40	1.00

Series II						
Sample	$\alpha/(\alpha+\beta)$[a]	GP vol.%[b]	Y_2O_3	Si_3N_4	AlN	Al_2O_3
G10B06	0	10	5.48	83.94	2.19	8.38
G10ABY20	0.2	10	6.62	81.84	3.66	7.96
G05ABY30	0.3	5	4.53	83.78	6.23	5.50
G10ABY30	0.3	10	7.13	80.80	4.48	7.68
G20ABY30	0.3	20	12.26	74.90	1.01	11.97
G10ABY50	0.5	10	8.28	78.66	6.09	7.05
G10ABY100	1.0	10	10.98	73.29	10.24	5.56

[a] Designed fraction of α.
[b] The designed amount of a secondary intergranular amorphous glass phase (GP) in volume percent.

A number of composites with nominal $\alpha/(\alpha+\beta)$ ratios fixed at 0, 0.2, 0.3, 0.5 and 1.0 were prepared. The balanced overall compositions thus fall along the A–B line shown in Fig. 1. In series II 5, 10 and 20 vol.% of a secondary glass-forming phase was added to the series-I compositions. The nominal composition of the glass-forming phase (added as a powder mixture) was $Y_{1.75}Si_{2.625}Al_{1.0}O_{7.5}N_{1.25}$ (28Y; 56Si; 16Al; 80O; 20N in equivalent%[1] of the cations and anions respectively).

Specimens were prepared from commercial Si_3N_4 (UBE, SN-E10), AlN (H.C. Starck-Berlin, grade B), Y_2O_3 (99.9%, Johnson Matthey Chemicals Ltd), and Al_2O_3 (Alcoa, A16SG), and corrections were made for the small amounts of oxygen present in the Si_3N_4 and AlN raw materials. The starting-material mixtures were milled in water-free propanol for 24 h in a plastic jar, using sialon-milling media. The dried powder mixtures were sintered in a hot pressing apparatus (Thermal Technology Inc.) at a temperature of 1750°C and a pressure of 30 MPa for 90 min. Three samples (B06, ABY20 and ABY30, see below), however, had to be sintered by means of the Spark Plasma Sintering (SPS) technique (Sumitomo coal mining company Ltd)[11] at 1700°C and at a pressure of 50 MPa for 5 min, in order to ensure densification.

2.2. Characterisation techniques

Densities were measured by use of Archimedes' principle. Before physical characterisation, the specimens were carefully polished by standard diamond polishing

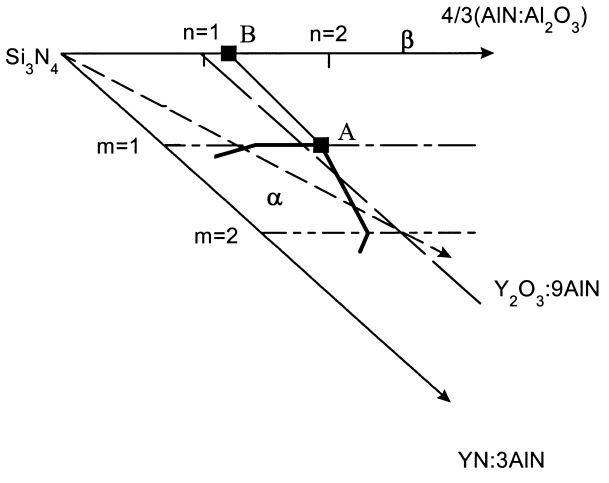

Fig. 1. The α–β plane of the phase diagram for Y–Si–Al–O–N sialon system with the balanced overall compositions marked on the line A–B.

techniques. The hardness (HV_{10}) and indentation fracture toughness (K_{1c}) at room temperature were determined using a Vickers diamond indenter with a 98 N load, and the fracture toughness was evaluated according to the method of Anstis et al.,[12] assuming a value of 300 GPa for Young's modulus for all compositions. Five indentations were made for each sample, and the average values for HV_{10} and K_{1c} are given with error bars.

The microstructures were examined in a scanning electron microscope (SEM, JEOL 880) equipped with an energy-dispersive spectrometer (EDS, LINK *ISIS*) that allows detection of boron and heavier elements. Micrographs of fractured surfaces were obtained in secondary electron mode (SE) and micrographs of polished samples were obtained in backscattered electron mode (BSE) at an acceleration voltage of 20 kV in order to obtain the best contrast. The amounts of glass phase in series II were evaluated with an image-analysing package supplied with the LINK *ISIS* system. For those analyses, images were collected at 10 and 15 kV acceleration voltages. The contrast difference between the α- and β-sialon phases and the yttrium-containing glass phase was used to estimate content of these phases in vol.%. The estimates of the minimum and maximum amount of glass phase gave an error of ±2%.

All samples were crushed and characterised by their X-ray powder diffraction (XRD) patterns obtained with a Guinier-Hägg focusing camera. CuK_α radiation ($\lambda = 1.5405981$ Å) was used, and powdered silicon ($a = 5.430879$ Å at 25°C) was added as an internal standard. The recorded films were evaluated with the computer programs SCANPI[13] and PIRUM.[14] The latter was used to determine the unit cell parameters for the different phases. The z value of the β-sialon phase was obtained from the unit cell dimensions of the samples, using the equations given by Ekström et al.,[15] see Table 2. The amounts of α- and β-sialon were estimated by comparison of the intensities of the two strongest XRD lines for the two phases (1 0 2 and 2 1 0 for α-sialon and 1 0 1 and 2 1 0 for β-sialon).

2.3. Thermal shock measurements

Cylindrical samples with a diameter of 12 mm and a thickness of 3.9±0.3 mm (see Table 3) were ground to make the two surfaces parallel, and one side was carefully polished. Well-defined cracks were initiated with a Vickers indenter. Four indents were made on each sample, and each indent generated four cracks (see Fig. 2), so that a total of 16 cracks were initiated on each sample. In order to compare different samples more easily, the original crack length was held constant, around 100 μm. As a consequence, different samples had to be indented with different loads (see Table 3). The crack length was measured in an optical microscope (Olympus PMG3). A vertical tubular furnace was heated to the preset starting temperature 190°C, which was then normally increased stepwise by 100°C. The sample was hoisted into the furnace and was thermally equilibrated for 20 min; then it was quenched into a 90°C thermostated water bath. The crack growth was measured at each temperature, and the total percentage growth was calculated which was then plotted versus the temperature difference (ΔT). It has earlier been shown that the same sample can be re-used for a whole quenching series.[9]

The test pieces were heated in air, but no severe oxidation was observed in the experiments presented below, as the test samples were not heated above 1000°C.[16] It was decided to use a 90°C water bath because of practical difficulties in keeping the water bath at the boiling point, due to vigorous steam production. The heat transfer is better at the boiling point, but even at 90°C the surface heat transfer is high compared to water at room temperature.[17]

3. Results and discussion

3.1. Phase compositions and microstructure

All samples were fully densified, and the measured densities are listed in Table 2. Conventional hot pressing could not densify three of the samples, B06, ABY20, and ABY30, most probably due to insufficient liquid phase being formed at the sintering temperatures used in this study. For those samples it was instead necessary to use SPS sintering in order achieve full density. This was confirmed by SEM investigation of fractured surfaces.

The phase composition, the $\alpha/(\alpha+\beta)$ ratio and the unit cell dimensions, based on XRD analysis, for both α- and β-sialon phases formed in all compacted samples are listed in Table 2. The phases formed in series I where basically α- and β-sialon with a very small amount of an unreacted residual α-Si_3N_4 phase in sample ABY50. Besides α- and β-sialon, the "B-phase" (Y_2SiAlO_5N) was identified in samples of series II which according to previous work most probably is crystallised from the residual intergranular amorphous phase during cooling.[18] In the present case the formation of a substantial amount of B-phase in samples of series II seems to indicate that the yttrium content designed for glass composition is somewhat too low. The α-phase content is lower than expected in these samples, implying that the formed glass phase has consumed more yttrium than nominally assigned to it.

The unit cell dimensions determined for the α-sialon are similar, indicating that compositions in all samples are close. The composition is, as expected, on the oxygen-rich boundary of the α-sialon-forming area facing

Table 2
The measured unit cell parameters, α/β-ratios, and amount of glass phase

Series I

Sample	Phase composition[a]	α-Sialon cell dimensions (Å)		β-Sialon cell dimensions (Å)			Measured α/(α+β) ratio	Measured density (g/cm^3)
		a	c	a	c	z value		
B06	β(s)	–	–	7.6178(3)	2.9187(2)	0.5	0	3.16
ABY20	β(s), α(w)	7.7548(140)	5.6618(200)	7.6212(3)	2.9198(2)	0.6	0.06	3.19
ABY30	β(s), α(m)	7.8002(130)	5.6940(230)	7.6206(4)	2.9200(2)	0.6	0.2	3.21
ABY50	β(s), α(w), α*(w)	7.7968(4)	5.6750(4)	7.6177(4)	2.9194(3)	0.5	0.5	3.21
ABY100	α(s), β(w)	7.8035(3)	5.6823(4)				1.0	3.26

Series II

Sample	Phase composition	α-Sialon cell dimensions (Å)		β-Sialon cell dimensions (Å)			Measured vol.% glass	Measured α/α+β ratio	Measured density
		a	c	a	c	z value		(wt.%)	(g/cm^3)
G10B06	β(s)	–	–	7.6207(2)	2.9201(1)	0.6	10	0	3.21
G10ABY20	β(s), b(w)	–	–	7.6245(3)	2.9216(2)	0.6	13	0	3.24
G05ABY30	β(s), α(m), b(w)	7.7952(9)	5.6790(7)	7.6238(6)	2.9214(4)	0.6	5	0.3	3.22
G10ABY30	β(s), α(w), b(w)	7.799(1)	5.677(0)	7.6247(4)	2.9225(2)	0.7	11	0.06	3.23
G20ABY30	β(s), b(m)	–	–	7.6241(4)	2.9208(2)	0.6	15	0	3.28
G10ABY50	β(s), α(m), b(m)	7.8010(4)	5.6829(4)	7.6256(3)	2.9223(2)	0.7	12	0.3	3.26
G10ABY100	α(s), β(w), b(w)	7.8066(3)	5.8668(3)	7.625(1)	2.921(0)	0.6	16	0.9	3.31

[a] α*, Residual α–Si_3N_4; α-, α-sialon; β, β-sialon; b, B-phase; XRD intensity: s, strong; m, medium; w, weak.

Table 3
Indentation load, sample thickness, initial crack length and critical thermal shock temperature

Sample	Sample thickness (mm)	Indentation load (N)	Initial crack length (μm)
B06	4.04	35	91
ABY20	4.04	45	86
ABY30	4.08	40	75
ABY50	3.86	63	114
ABY100	3.61	67	117
G10B06	4.16	60	98
G10ABY20	3.88	70	120
G05ABY30	3.39	58	95
G10ABY30	4.19	50	78
G20ABY30	3.43	65	94
G10ABY50	4.17	55	106
G10ABY100	3.79	65	96

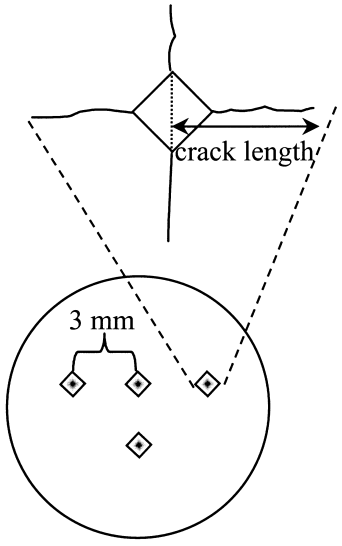

Fig. 2. Positioning of the indents on the sample and the definition of crack length.

to the β-sialon line, in accordance with previous findings. The z values calculated from unit cell dimensions for β-sialon are very close to the designed one, i.e. 0.6, confirming the previous results and that this is a β-sialon composition that is in equilibrium with the α-sialon.[10]

Some selected SEM micrographs of the samples with and without glass addition are shown in Fig. 3a–f. The β-sialon phase is black, while α-sialon is grey because it contains the heavy element yttrium, the B-phase and the glass phase both appear white. The following microstructural features can be observed;

1. The samples in series I contain almost no glass phase.
2. The samples are all fully densified.
3. β-Sialon grains have a higher aspect ratio than α-sialon grains when a glass phase is present.

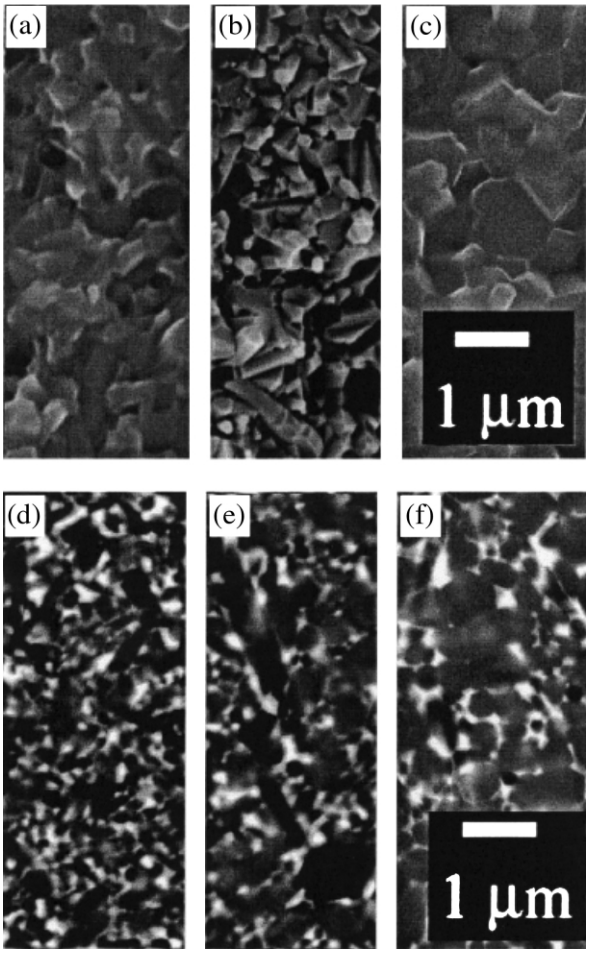

Fig. 3. SEM micrographs of fractured surfaces of (a) ABY30, (b) ABY50, (c) ABY100, and back-scattered micrographs of polished surfaces of (d) G10ABY30, (e) G10ABY50, and (f) G10ABY100.

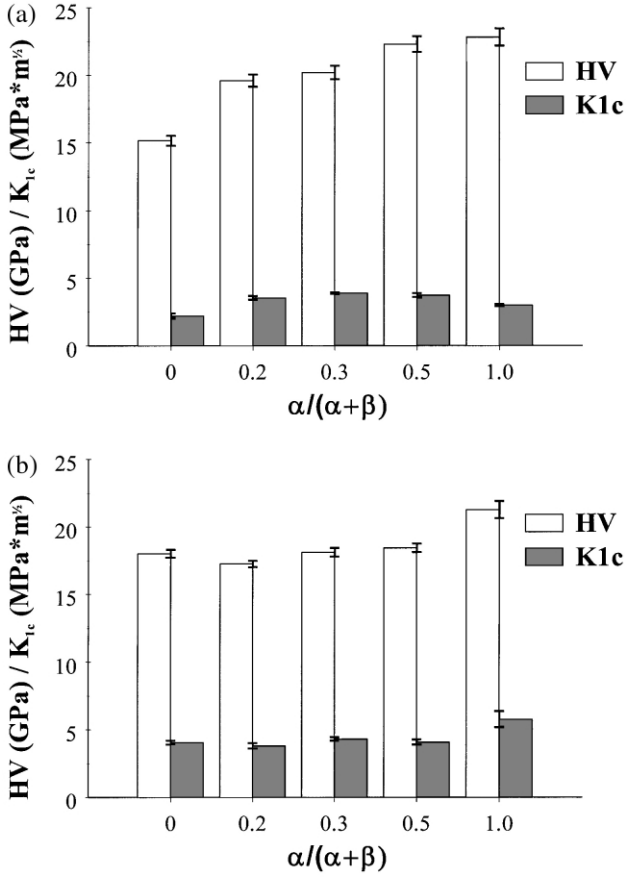

Fig. 4. Hardness (HV) and fracture toughness (K_{1c}) versus the $\alpha/(\alpha+\beta)$-ratio for samples (a) without and (b) with 10% extra glass addition.

3.2. Hardness and fracture toughness

The Vickers hardness and fracture toughness values determined are plotted versus the nominal $\alpha/(\alpha+\beta)$-ratio in Fig. 4a–b. Similar to previous observations[3] the optimum combination of hardness and fracture toughness is obtained with an $\alpha/(\alpha+\beta)$-ratio of around 0.5 for samples in series I. A more general tendency is that the hardness increases with increasing α-sialon content. Addition of 10 vol.% glass decreases the hardness and increases fracture toughness values for all compositions. The quantitative influence of the amount of added glass phase on the hardness and fracture toughness is shown in Fig. 5, where hardness and fracture toughness of a series of samples with a fixed $\alpha/(\alpha+\beta)$-ratio value of 0.3 are plotted versus the amount of extra glass addition.

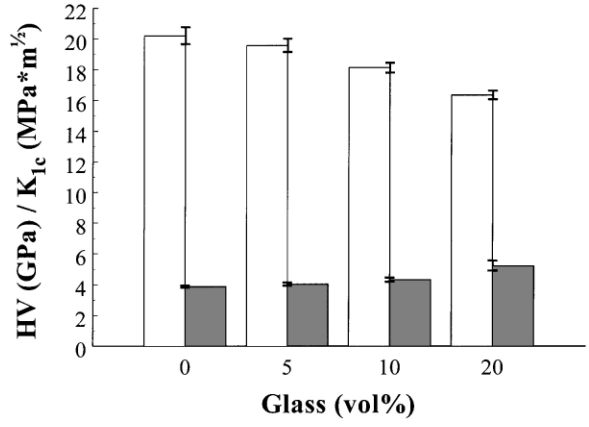

Fig. 5. Hardness (HV) and fracture toughness (K_{1c}) versus the amount of extra glass addition when $\alpha/(\alpha+\beta)$-ratio is fixed at 30%.

3.3. Thermal shock properties

The crack extension versus the thermal-shock temperature difference for samples in series I is shown in Fig. 6a. The thermal shock properties are highly dependent on the α/β-ratio. The best thermal shock resistance was found at a low fraction of α. Increasing the fraction of α-phase decreases the thermal shock resistance, and the pure α-sialon clearly has the poorest thermal shock behaviour of all samples in the two series.

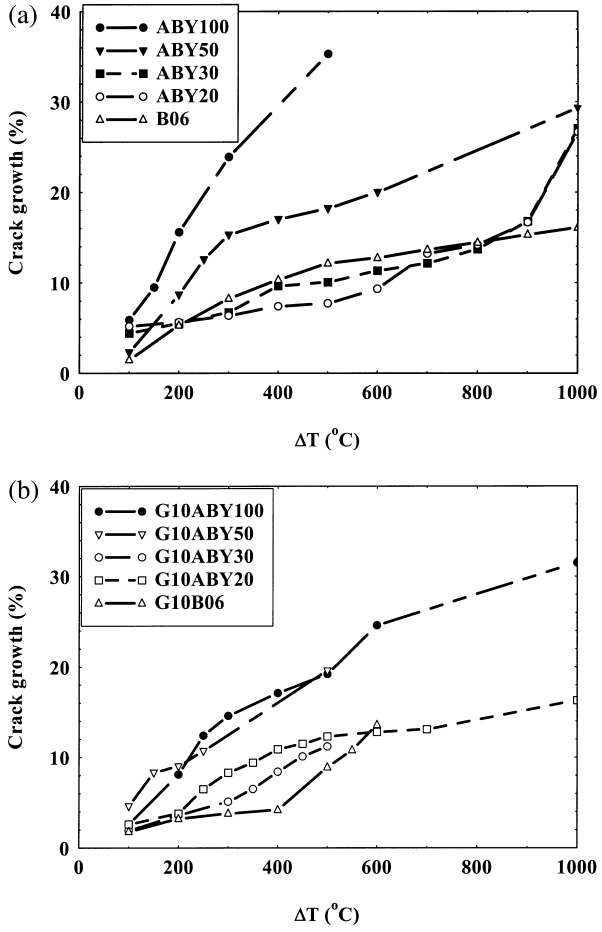

Fig. 6. Crack growth in percentage versus the temperature difference (ΔT) for α/β-sialons with different z values: (a) without glass and (b) with 10% glass.

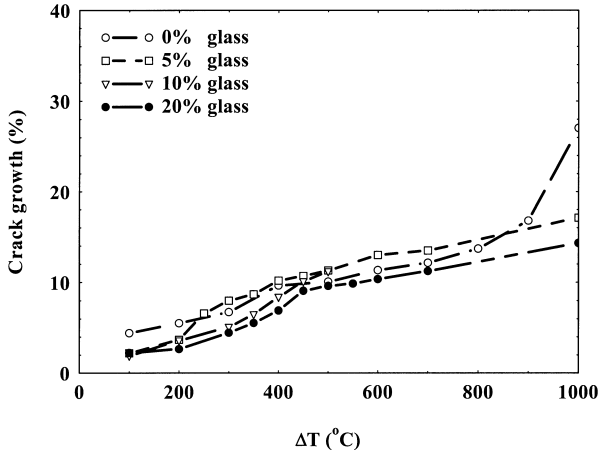

Fig. 7. Crack growth in percentage versus the temperature difference for α/β-sialons with 30% α and varying amounts of glass phase.

It is not only the ratio of the different phases α and β that determine the thermal shock properties, the morphology of the phases may also influence. The α-phase is equiaxed while the β-phase is elongated. A possible explanation for that samples with a low fraction of α-sialon shows better thermal shock behaviour is that most of the β-sialon grains are elongated in those samples. Elongated grains seem to improve the thermal shock behaviour of these materials by providing energy consuming mechanisms such as crack-deflection and/or bridging to hinder the crack extension.

The presence of a residual grain-boundary glassy phase slightly improves the thermal shock resistance (*cf*. Fig. 6a and b). The influence of the amount of glass added to a sialon with nominal composition $\alpha/(\alpha+\beta)=0.3$ is shown in Fig. 7. The best thermal shock resistance is found for the sample with the highest glass content investigated. One explanation for this could be that the presence of a glassy phase, which is a liquid at high temperatures, enhances the grain growth, so that more elongated grains with high aspect ratio are formed.

Another important factor that may influence the thermal shock resistance of a material is the thermal conductivity. Very little is published about the thermal conductivity for α-, β-, and α/β-sialon ceramics (with or without addition of an extra glass phase). A previous investigation on silicon nitride ceramics, however, reveals that the thermal conductivity of β-Si_3N_4 increases about 3 times when the grain size increases from ~1 to ~5 μm.[19] If the same tendency is valid also for our materials one would expect that the α/β sialons prepared without addition of extra glass phase and having a fine grained microstructure, would exhibit a lower thermal conductivity and not as good thermal shock resistance as materials prepared with addition of extra glass, i.e. materials having a more coarse grained microstructure. In fact, our measurements do show such a tendency, indicating that knowledge of the thermal conductivity of the materials is of importance in order to explain the thermal shock behaviour.

Andersson and Rowcliffe[8] defined a critical thermal shock temperature (ΔT_c) as the temperature where 25% of the cracks have grown more than 10% of their original length. We found that almost all our thermal shock curves could be divided into three different groups based on the slope of the crack growth versus temperature difference (ΔT) curve. One group (Type I) represent curves were there is a slow increase of crack length with increasing ΔT over the whole temperature interval investigated. For Type III the cracks grow rapidly with increasing ΔT. The Type II materials behave as Type I at low ΔT, but changes into Type III behaviour above some critical temperature.

The β-sialons are of Type I and are thus suitable for high temperature applications. The α/β-sialons are of Type II and can only be used below some critical ΔT value. The α-sialons are of Type III as the cracks grow more than 10% at very low ΔT values and are thus not suitable for high temperature applications.

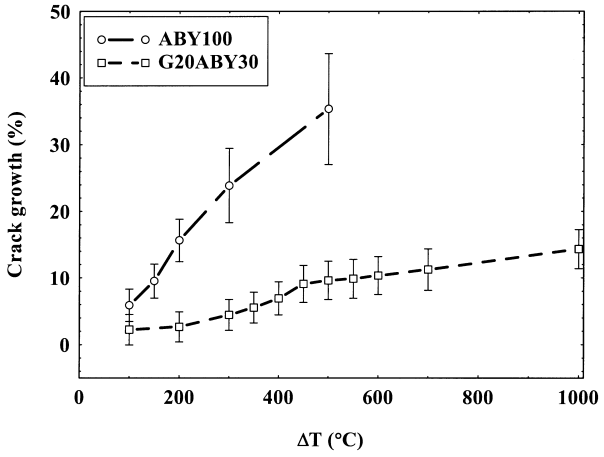

Fig. 8. The crack growth in percentage versus the temperature difference for two sialon materials that have different thermal shock behaviour. The standard deviation is low and almost constant for a Type I material (G20ABY30) while the standard deviation increase with increasing ΔT for a Type III material (ABY100).

The standard deviation measured for the crack growth can also be used to illustrate different types of thermal shock behaviour. A Type I curve shows a low standard deviation that is about the same over the whole temperature interval measured. On the other hand a Type III curve show increasing standard deviations with increasing ΔT (see Fig. 8). The fact that the standard deviation increases with increasing ΔT suggest that the crack growth is uncontrolled.

4. Conclusions

An indentation-quench method based on Vickers cracks for measuring thermal-shock properties has been applied to mixed α/β-sialon materials. The percentage crack growth is measured at each heating-quenching step, and the statistics are improved by making several Vickers indents on the same sample.

The z value of the β-phase was held constant at 0.6, and the α-phase ($Y_xSi_{12-(m+n)}Al_{m+n}O_nN_{16-n}$) had a composition of $x=0.33$, $m=1.0$, and $n=1.2$. The thermal shock resistance improves with increasing fraction of β-phase and with increasing amount of yttrium-containing glass phase.

Acknowledgements

This work has been performed within the Inorganic Interfacial Engineering Centre, supported by the Swedish National Board for Industrial and Technical Development (NUTEK) and the following industrial partners: Erasteel Kloster AB, Ericsson Cables AB, Höganäs AB, Kanthal AB, OFCON Optical Fiber Consultants AB, Sandvik AB, Seco Tools AB and Uniroc AB.

References

1. Ekström, T. and Nygren, M., Sialon ceramics. *J. Am. Ceram. Soc.*, 1992, **75**, 259–276.
2. Ekström, T., Falk, L. and Shen, Z., Duplex α-β SiAlON ceramics stabilized by dysprosium and samarium. *J. Am. Ceram. Soc.*, 1997, **80**, 301–312.
3. Falk, L. K. L., Shen, Z. and Ekström, T., Microstructral stability of duplex α-β sialon ceramics. *J. Eur. Ceram. Soc.*, 1997, **17**, 1099–1112.
4. Buessem, W. R., *J. Am. Ceram. Soc.*, 1955, **38**, 15.
5. Kingery, W. D., Factors affecting thermal stress resistance of ceramic materials. *J. Am. Ceram. Soc.*, 1955, **38**, 3–15.
6. Davidge, R. W. and Tappin, G., Thermal shock and fracture in ceramics. *Trans. Br. Ceram. Soc.*, 1967, **66**, 405–422.
7. Hasselman, D. P. H., Strength behaviour of polycrystalline alumina subjected to thermal shock. *J. Am. Ceram. Soc.*, 1970, **53**, 490–494.
8. Andersson, T. and Rowcliffe, D. J., Indentation thermal shock test for ceramics. *J. Am. Ceram. Soc.*, 1996, **79**, 1509–1514.
9. Pettersson, P., Shen, Z., Johnsson, M. and Nygren, M., Thermal shock properties of β-sialon ceramics. Submitted to *J. Am. Ceram. Soc.*
10. Shen, Z. and Nygren, M., On the extension of the α-sialon phase area in yttrium and rare-earth doped systems. *J. Eur. Ceram. Soc.*, 1997, **17**, 1639–1645.
11. Tokita, M., Mechanism of spark plasma sintering and its application to ceramics. *Nyu Seramikkusu*, 1997, **10**, 43.
12. Anstis, G. R., Chantikul, P., Lawn, B. R. and Marshall, D. B., A critical evaluation of indentation techniques for measuring fracture toughness: I, Direct crack measurements. *J. Am. Ceram. Soc.*, 1981, **664**, 533–538.
13. Johansson, K. E., Palm, T. and Werner, P. E., An automatic microdensiometer for X-ray diffraction photographs. *J. Phys. E. Sci. Instrum.*, 1980, **13**, 1289–1291.
14. Werner, P. E., A FORTRAN program for least-squares refinement of crystal structure cell dimensions. *Arkiv Kemi*, 1969, **31**, 513–516.
15. Ekström, T., Käll, P. O., Nygren, M. and Olsson, P. O., Dense single phase β-sialon ceramics by glass encapsulated hot isostatic pressing. *J. Mater. Sci.*, 1989, **24**, 1853–1861.
16. Ramesh, R., Pomeroy, M. J., Chu, H. and Datta, P. K., Effect of gaseous environment on the corrosion of β-sialon materials. *J. Eur. Ceram. Soc.*, 1995, **15**, 1007–1014.
17. Becher, P. F., Effect of water bath temperature on the thermal shock of Al_2O_3. *J. Am. Ceram. Soc.*, 1981, **64**, C17– C18.
18. Mandal, H., Thompson, D. P. and Ekström, T., Reversible α-β sialon transformation in heat-treated sialon ceramics. *J. Eur. Ceram. Soc.*, 1993, **12**, 421–429.
19. Kitayama, M., Hirao, K., Toriyama, M. and Kanzaki, S., Thermal conductivity of β-Si_3N_4: I, Effects of various microstructural factors. *J. Am. Ceram. Soc.*, 1999, **82**, 3105–3112.